Inorg. Chem. **2006**, *45*, 9434–9441

Computational Studies on the Photophysical Properties and NMR Fluxionality of the Tetranuclear Copper(I) Complexes $[Cu_4(\mu\text{-dppm})_4(\mu_4\text{-E})]^{2+}$ (E = PPh and S)

Wai Han Lam, Eddie Chung-Chin Cheng, and Vivian Wing-Wah Yam*

Centre for Carbon-Rich Molecular and Nano-Scale Metal-Based Materials Research and the Department of Chemistry, The University of Hong Kong, Pokfulam Road, Hong Kong SAR, People's Republic of China

Received July 12, 2006

Density functional theory (DFT) calculations at the hybrid Perdew, Burke, and Ernzerhof functional level were performed to study the electronic structures of the ground and excited states of the luminescent tetranuclear copper(I) complexes $[Cu_4(\mu\text{-dppm})_4(\mu_4\text{-E})]^{2+}$ [E = PPh (**1**) and S (**2**)] by using model complexes $[Cu_4(\mu\text{-}H_2PCH_2PH_2)_4(\mu_4\text{-E})]^{2+}$ [E = PPh (**1a**) and S (**2a**)]. The time-dependent DFT method at the same level associated with the conductor-like polarizable continuum model was used to study the nature of the low-energy transitions in their electronic absorption spectra. The results indicate that the lowest energy absorptions of both **1** and **2** are attributed to ligand-to-metal charge-transfer (LMCT) (E → Cu_4) with mixing of metal-cluster-centered (MCC) (3d → 4s/3d → 4p) singlet–singlet transitions. The geometry optimizations on the lowest energy triplet state reveal that the emissive states of both complexes involve a considerable structural distortion in which they are derived predominantly from an admixture of ^{3}LMCT (E → Cu_4) and ^{3}MCC (3d → 4p) origin. In addition to the photophysical properties, the fluxional behavior of **2** observed from the NMR studies but not that of **1** was investigated. It is found that the fluxionality in **2** involves the shuttling of the sulfido ligand through the rectangular Cu_4 core.

Introduction

It is well-known that polynuclear d^{10} complexes such as those of copper(I), silver(I), and gold(I) possess remarkable photophysical and photochemical properties.[1−8] Recently, we reported the synthesis and structural characterization of a novel luminescent tetranuclear copper(I) phosphinidene complex, $[Cu_4(\mu\text{-dppm})_4(\mu_4\text{-PPh})](BF_4)_2$ (**1**·$(BF_4)_2$) (dppm = bis(diphenylphosphanyl)methane).[9] An analogue complex, $[Cu_4(\mu\text{-dppm})_4(\mu_4\text{-S})](PF_6)_2$ (**2**·$(PF_6)_2$), was also synthesized earlier by our group and was also found to possess rich luminescent properties.[8a]

* To whom correspondence should be addressed. E-mail: wwyam@hku.hk. Fax: +(852) 2857-1586. Tel: +(852) 2859-2153.

(1) (a) Ford, P. C.; Vogler, A. *Acc. Chem. Res.* **1993**, *26*, 220−226. (b) Ford, P. C.; Cariati, E.; Bourassa, J. *Chem. Rev.* **1999**, *99*, 3625−3647. (c) Yam, V. W.-W.; Lo, K. K.-W. *Chem. Soc. Rev.* **1999**, 323−334.

(2) (a) Kyle, K. R.; Ryu, C. K.; DiBenedetto, J. A.; Ford, P. C. *J. Am. Chem. Soc.* **1991**, *113*, 2954−2965. (b) Vitale, M.; Palke, W. E.; Ford, P. C. *J. Phys. Chem.* **1992**, *96*, 8329−8336. (c) Sabin, F.; Ryu, C. K.; Ford, P. C.; Vogler, A. *Inorg. Chem.* **1992**, *31*, 1941−1945. (d) Ford, P. C. *Coord. Chem. Rev.* **1994**, *132*, 129−140.

(3) (a) Vogler, A.; Kunkely, H. *J. Am. Chem. Soc.* **1986**, *108*, 7211−7212. (b) Vogler, A.; Kunkely, H. *Chem. Phys. Lett.* **1988**, *150*, 135−137. (c) Vogler, A.; Kunkely, H. *Chem. Phys. Lett.* **1989**, *158*, 74−76.

(4) (a) Avdeef, A.; Fackler, J. P., Jr. *Inorg. Chem.* **1978**, *17*, 2182−2187. (b) Khan, M. N. I.; Fackler, J. P., Jr.; King, C.; Wang, J. C.; Wang, S. *Inorg. Chem.* **1988**, *27*, 1672−1673. (c) King, C.; Wang, J. C.; Khan, M. N. I.; Fackler, J. P., Jr. *Inorg. Chem.* **1989**, *28*, 2145−2149. (d) Forward, J. M.; Bohmann, D.; Fackler, J. P., Jr.; Staples, R. J. *Inorg. Chem.* **1995**, *34*, 6330−6336.

(5) (a) Barrie, J. D.; Dunn, B.; Hollingsworth, G.; Zink, J. I. *J. Phys. Chem.* **1989**, *93*, 3958−3963. (b) Shin, K. S. K.; Barrie, J. D.; Dunn, B.; Zink, J. I. *J. Am. Chem. Soc.* **1990**, *112*, 5701−5706. (c) Henary, M.; Zink, J. I. *Inorg. Chem.* **1991**, *30*, 3111−3112. (d) Hanna, S. D.; Zink, J. I. *Inorg. Chem.* **1996**, *35*, 297−302.

(6) (a) Che, C.-M.; Kwong, H.-L.; Yam, V. W.-W.; Cho, K.-C. *J. Chem. Soc., Chem. Commun.* **1989**, 885−886. (b) Che, C.-M.; Kwong, H.-L.; Poon, C.-K.; Yam, V. W.-W. *J. Chem. Soc., Dalton Trans.* **1990**, 3215−3219. (c) Yam, V. W.-W.; Cheng, E. C.-C.; Zhu, N. *Angew. Chem., Int. Ed.* **2001**, *40*, 1763−1765.

(7) (a) Yam, V. W.-W.; Fung, W. K.-M.; Cheung, K.-K. *Angew. Chem., Int. Ed. Engl.* **1996**, *35*, 1100−1102. (b) Yam, V. W.-W.; Choi, S. W.-K.; Chan, C.-L.; Cheung, K.-K. *Chem. Commun.* **1996**, 2067−2068.

(8) (a) Yam, V. W.-W.; Lee, W.-K.; Lai, T.-F. *J. Chem. Soc., Chem. Commun.* **1993**, 1571−1573. (b) Yam, V. W.-W.; Lo, K. K.-W.; Cheung, K.-K. *Inorg. Chem.* **1996**, *35*, 3459−3462. (c) Yam, V. W.-W.; Lo, K. K.-W.; Wang, C.-R.; Cheung, K.-K. *Inorg. Chem.* **1996**, *35*, 5116−5117.

(9) Yam, V. W.-W.; Cheng, E. C.-C.; Zhu, N. *Chem. Commun.* **2001**, 1028−1029.

10.1021/ic0612855 CCC: $33.50
Published on Web 10/11/2006

Scheme 1. Structure of **1** and **2**

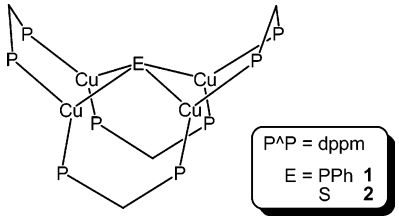

Complex cations **1** and **2** adopt a similar structure in which the four copper atoms are arranged almost on the same plane to form a rectangular array, with the four bridging dppm ligands in a saddle-like configuration (Scheme 1). Both the phosphorus atom of the phosphinidene ligand and the sulfur atom in **1** and **2**, respectively, sit at the apex of the distorted square pyramid and quadruply bridge the four copper atoms, with projection above the idealized Cu_4 plane. The Cu−Cu distances range from 2.823 to 3.446 Å in **1** and from 2.868 to 3.128 Å in **2**, which show no significant Cu···Cu interaction.

Excitation of **1** in the solid state and in fluid solutions resulted in intense long-lived red luminescence, while **2** gave a higher energy emission with yellow-orange luminescence both in the solid state and in fluid solutions. On the basis of the observed emission energy trends and previous ab initio calculation at the Hartree−Fock (HF) level of theory on $[Cu_4(\mu\text{-}H_2PCH_2PH_2)_4(\mu_4\text{-}E)]^{2+}$ (E = S and Se)[10a] as well as both HF and Fenske−Hall calculations on related tetranuclear silver(I) chalcogenide systems,[10b,c] the emission of **1** and **2** was tentatively assigned to originate predominantly from the triplet state derived mainly from the ligand-to-metal charge-transfer (LMCT) [PPh or S → Cu] character with mixing of a metal-centered (MC) [3d → 4s/3d → 4p] Cu(I) state.

The two complexes differ not only in their photophysical properties, but also in the fluxional behavior in solution. The $^{31}P\{^1H\}$ NMR spectrum of **1** in CD_2Cl_2 showed two signals for the bridging diphosphine ligands at ambient temperature, corresponding to the two sets of diphosphines, namely, the upper sets (on the same side as the PPh ligand) and the lower sets (on the opposite side of the PPh ligand) of bridging diphosphines. However, only one signal for the diphosphine ligands was observed in **2** both at 298 and at 233 K in acetone-*d*.[6] All these suggest that there is a rapid exchange of the upper and lower sets of bridging diphosphines in **2**, but not in **1**.

Density functional theory (DFT) calculation has been successfully applied in the elucidation and prediction of a broad range of properties of transition-metal complexes, because of its relatively low computational cost with reasonable accuracy.[11a] More recently, time-dependent DFT (TDDFT) has been widely used for the prediction of optical spectra of transition-metal complexes.[11b] Several studies have pointed out that TDDFT would give better agreement with experiments for excitation energies of low-lying excited states than those obtained by the configuration interaction singles (CIS) approach.[12] In view of the rich luminescence properties and the potential application as optoelectronic materials of these tetranuclear copper complexes, DFT calculations at the PBE1PBE level have been undertaken in this work to study the electronic structures of the ground and excited states of **1** and **2** to gain a better understanding of the spectroscopic origin of and the effect of the apical ligand on the emission properties, as well as to provide insight into the extent of the distortion in the excited states relative to that of the ground states. Furthermore, the TDDFT method at the same level associated with the conductor-like polarizable continuum model (CPCM) was used to study the nature of the low-energy transitions in their electronic absorption spectra. It was pointed out that the inclusion of the solvent environment in TDDFT calculations could have a more realistic description of charge-transfer electronic transitions.[13] Although the electronic structure of **2a** was studied previously at different levels of calculation, the excited-state calculations on **2a** have not been explored.

In addition to the photophysical properties, the difference in the fluxionality of **1** and **2** observed will be rationalized by a computational study on the mechanism of exchange between the upper and lower bridging diphosphines in **2**. Two possible mechanisms will be studied. One involves the shuttling process of the sulfido atom through the rectangular Cu_4 core (Scheme 2a). Via this pathway, the chemical environments of the two types of diphosphines can be exchanged without involving any flipping motion of the diphosphine ligands. Another pathway is believed to involve the up−down flipping motion of the two pairs of diphosphines (Scheme 2b).

Computational Details

Calculations were carried out using the Gaussian03 software package.[14] To reduce the computational cost, model complexes $[Cu_4(\mu\text{-}H_2PCH_2PH_2)_4(\mu_4\text{-}PPh)]^{2+}$ (**1a**) and $[Cu_4(\mu\text{-}H_2PCH_2PH_2)_4(\mu_4\text{-}S)]^{2+}$ (**2a**) were used to mimic the complexes $[Cu_4(\mu\text{-dppm})_4(\mu_4\text{-}PPh)]^{2+}$ (**1**) and $[Cu_4(\mu\text{-dppm})_4(\mu_4\text{-}S)]^{2+}$ (**2**), respectively. DFT at the hybrid Perdew, Burke, and Ernzerhof functional (PBE1PBE) level[15] was used to optimize the ground state of **1a** and **2a** and the transition states for the diphosphine exchange. The unrestricted UPBE1PBE was used to optimize the low-lying triplet states of **1a** and **2a**. Vibrational frequencies were calculated for all stationary points to verify that each was a minimum (NIMAG = 0) or a transition state (NIMAG = 1) on the potential energy surface. To make a comparison with the DFT result, a geometry optimization of **2a** using the second-order Møller−Plesset (MP2) level of theory[16] with the constraint of C_{2v} symmetry was also performed.

(10) (a) Wang, C.-R.; Lo, K. K.-W.; Fung, W. K.-M.; Yam, V. W.-W. *Chem. Phys. Lett.* **1998**, *296*, 505−514. (b) Wang, C.-R.; Lo, K. K.-W.; Yam, V. W.-W. *J. Chem. Soc., Dalton Trans.* **1997**, 227−230. (c) Wang, C.-R.; Lo, K. K.-W.; Yam, V. W.-W. *Chem. Phys. Lett.* **1996**, *262*, 91−96.

(11) (a) Noodleman, L.; Lovell, T.; Han, W.-G.; Liu, T.; Torres, R. A.; Himo, F. In *Comprehensive Coordination Chemistry II*; McCleverty, J. A., Meyer, T. J., Eds.; Elsevier: Amsterdam, 2004; Vol. 2, pp 491−510. (b) Van Gisbergen, S. J. A.; Baerends, E. J. In *Comprehensive Coordination Chemistry II*; McCleverty, J. A., Meyer, T. J., Eds.; Elsevier: Amsterdam, 2004; Vol. 2, pp 511−517.

(12) (a) Jamorski, C.; Casida, M. E.; Salahub, D. R. *J. Chem. Phys.* **1996**, *104*, 5134−5147. (b) Hirata, S.; Head-Gordon, M. *Chem. Phys. Lett.* **1999**, *302*, 375−382. (c) Šeda, J.; Burda, J. V.; Brázdová, V.; Kapsa, V. *Int. J. Mol. Sci.* **2004**, *5*, 196−213.

(13) (a) Vlèek A., Jr.; Záliš, S. *J. Phys. Chem. A* **2005**, *109*, 2991−2992. (b) Villegas J. M.; Stoyanov, S. R.; Reibenspies, J. H.; Rillema, D. P.; *Organometallics* **2005**, *24*, 395−404.

Scheme 2. Two Proposed Mechanisms for the Diphosphine Exchange in **2a**: (a) Shuttling Motion of the Sulfido Ligand and (b) Up−Down Flipping Motion of the Diphosphine Ligands

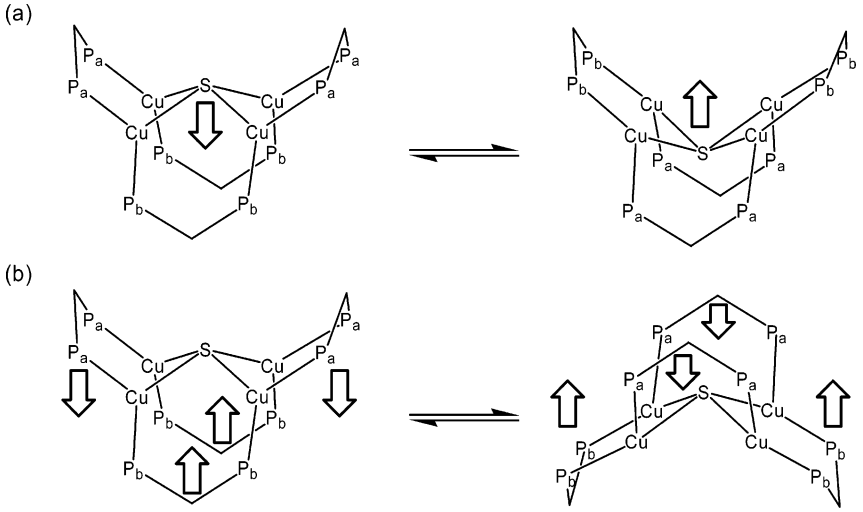

The Stuttgart effective core potentials (ECPs)[17] on Cu replaced the inner core electrons, and the associated basis set was applied to describe the outer core $[(3s)^2(3p)^6]$ and the valence 3d electrons. To increase the accuracy, an f polarization function ($\zeta_f(Cu) = 3.525$) was employed for Cu.[18] The 6-311G(d) basis set[19] was used for S and P atoms, while 6-31G(d)[20] was employed for C and H atoms.

Nonequilibrium TDDFT[21]/CPCM[22] calculations using the basis set previously described with the PBE1PBE functional were employed to produce the low-lying singlet and triplet excited states of **1a** and **2a** (CH_2Cl_2 as the solvent), on the basis of their corresponding singlet ground-state optimized geometries in the gas phase. Natural bond order (NBO)[23] calculations using the same basis sets and level of theory were performed on the optimized geometries of **1a** and **2a**.

Results and Discussion

Optimized Geometries. Selected structural parameters of the PBE1PBE-optimized geometries of **1a** are shown in Figure 1, together with the crystallographic data of **1** for comparison. Complex **1a** exhibits approximate C_{2v} symmetry in which the four copper atoms form a rectangular base and the phosphinidene ligand situates above the Cu_4 plane. The plane of the phenyl ring on the phosphinidene lies perpendicular to the Cu_4 plane and has an orientation that bisects the two longer Cu−Cu edges, Cu(1)−Cu(1′) and Cu(2)−Cu(2′).

In general, the calculated structural parameters are in good agreement with the experimental values. The shorter distance of Cu(1)−Cu(2) (2.911 Å) than Cu(1)−Cu(1′) (3.270 Å), the larger bond angle of Cu(1′)−Cu(1)−P(1) (141.5°) than Cu(2)−Cu(1)−P(3) (126.7°), and the longer bond distance of Cu(1)−P(1) (2.310 Å) than Cu(1)−P(3) (2.283 Å), which resulted from steric overcrowding among the phosphinidene moiety and the two upper bridging diphosphines in **1a**, were also reproduced.

Figure 1 shows the optimized geometry of **2a**, which also exhibits approximate C_{2v} symmetry with two long and two short Cu−Cu edges forming a rectangular base. The longer distances of Cu(1)−Cu(1′) and Cu(2)−Cu(2′) in **1a** than those in **2a** are in line with the larger bulk of the phosphinidene ligand, which results in a larger steric repulsion. Interestingly, the Cu(1)−Cu(2) and Cu(1′)−Cu(2′) distances in **1a** (2.911 Å) are calculated to be shorter than those in **2a** (2.966 Å), in agreement with the experimental structures of **1** and **2**, in which the average Cu−Cu distances of the two shorter Cu−Cu edges in **1** and **2** are 2.852 and 2.869 Å, respectively. Such a difference can be readily attributed to the greater $Cu^I\cdots Cu^I$ repulsive interaction in **2**. Since S is more electronegative than P, the Cu centers in **2** should carry

(14) Frisch, M. J.; Trucks, G. W.; Schlegel, H. B.; Scuseria, G. E.; Robb, M. A.; Cheeseman, J. R.; Montgomery, J. A., Jr.; Vreven, T.; Kudin, K. N.; Burant, J. C.; Millam, J. M.; Iyengar, S. S.; Tomasi, J.; Barone, V.; Mennucci, B.; Cossi, M.; Scalmani, G.; Rega, N.; Petersson, G. A.; Nakatsuji, H.; Hada, M.; Ehara, M.; Toyota, K.; Fukuda, R.; Hasegawa, J.; Ishida, M.; Nakajima, T.; Honda, Y.; Kitao, O.; Nakai, H.; Klene, M.; Li, X.; Knox, J. E.; Hratchian, H. P.; Cross, J. B.; Bakken, V.; Adamo, C.; Jaramillo, J.; Gomperts, R.; Stratmann, R. E.; Yazyev, O.; Austin, A. J.; Cammi, R.; Pomelli, C.; Ochterski, J. W.; Ayala, P. Y.; Morokuma, K.; Voth, G. A.; Salvador, P.; Dannenberg, J. J.; Zakrzewski, V. G.; Dapprich, S.; Daniels, A. D.; Strain, M. C.; Farkas, O.; Malick, D. K.; Rabuck, A. D.; Raghavachari, K.; Foresman, J. B.; Ortiz, J. V.; Cui, Q.; Baboul, A. G.; Clifford, S.; Cioslowski, J.; Stefanov, B. B.; Liu, G.; Liashenko, A.; Piskorz, P.; Komaromi, I.; Martin, R. L.; Fox, D. J.; Keith, T.; Al-Laham, M. A.; Peng, C. Y.; Nanayakkara, A.; Challacombe, M.; Gill, P. M. W.; Johnson, B.; Chen, W.; Wong, M. W.; Gonzalez, C.; Pople, J. A. *Gaussian 03*, revision C.02; Gaussian, Inc.: Wallingford, CT, 2004.
(15) (a) Ernzerhof, M.; Scuseria, G. E. *J. Chem. Phys.* **1999**, *110*, 5029−5036. (b) Ernzerhof, M.; Perdew, J. P.; Burke, K. *Int. J. Quantum Chem.* **1997**, *64*, 285−295.
(16) Møller, C.; Plesset, M. S. *Phys. Rev.* **1934**, *46*, 618.
(17) Dolg, M.; Wedig, U.; Stoll H.; Preuss, H. *J. Chem. Phys.* **1987**, *86*, 866−872.
(18) Ehlers, A. W.; Böhme, M.; Dapprich, S.; Gobbi, A.; Höllwarth, A.; Jonas, V.; Köhler, K. F.; Stegmann, R.; Veldkamp, A.; Frenking, G. *Chem. Phys. Lett.* **1993**, *208*, 111−114.
(19) McLean, A. D.; Chandler, G. S. *J. Chem. Phys.* **1980**, *72*, 5639−5648.
(20) Hariharan, P. C.; Pople, J. A. *Theor. Chim. Acta* **1973**, *28*, 213−222.
(21) (a) Stratmann, R. E.; Scuseria, G. E.; Frisch, M. J. *J. Chem. Phys.* **1998**, *109*, 8218−8224. (b) Bauernschmitt, R.; Ahlrichs, R. *Chem. Phys. Lett.* **1996**, *256*, 454−464. (c) Casida, M. E.; Jamorski, C.; Casida, K. C.; Salahub, D. R. *J. Chem. Phys.* **1998**, *108*, 4439−4449.
(22) (a) Barone, V.; Cossi, M. *J. Phys. Chem. A* **1998**, *102*, 1995−2001. (b) Cossi, M.; Rega, N.; Scalmani, G.; Barone, V. *J. Comput. Chem.* **2003**, *24*, 669−681.
(23) (a) Glendening, E. D.; Reed, A. E.; Carpenter, J. E.; Weinhold. F. *NBO*, version 3.1, Theoretical Chemistry Institute, University of Wisconsin, Madison. (b) Reed, A. E.; Curtiss, L. A.; Weinhold, F. *Chem. Rev.* **1988**, *88*, 899−926. (c) Weinhold, F.; Carpenter, J. E. *The Structure of Small Molecules and Ions*; Plenum Press: New York, 1988; p 227.

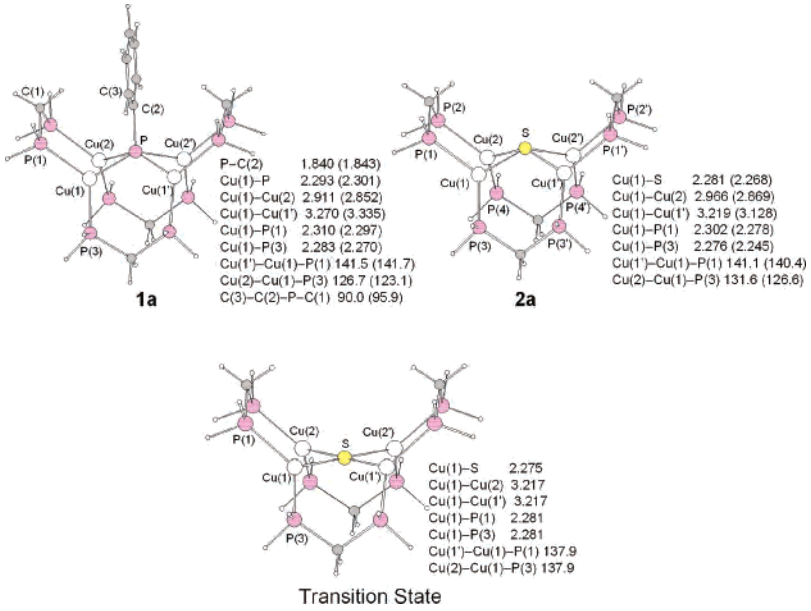

Figure 1. Selected structural parameters for **1a** and **2a** (with the experimental structural parameters of **1** and **2** in parentheses) and the transition state for the diphosphine exchange in **2a** involving the shuttling of the sulfido ligand optimized at the PBE1PBE level of theory. The distances and angles are in angstroms and degrees, respectively.

more positive charges, giving rise to greater $Cu^{I}\cdots Cu^{I}$ repulsion. Indeed, the calculated charges of the Cu atoms, on the basis of the NBO analyses, in the optimized structures of **1a** and **2a** are +0.57 and +0.59, respectively, supporting the repulsion argument. Similar arguments have been used to account for the difference of the Cu···Cu distances in cubic clusters $[Cu_8(\mu_8\text{-Se})\{S_2P(OEt)_2\}_6]$ and $[Cu_6\{S_2P(OEt)_2\}_6]$.[24]

The calculated Cu−Cu distances in **1a** and **2a** are found to somehow slightly deviate from the average experimental distances in **1** and **2**, respectively, compared with all other calculated bond distances. This discrepancy might be attributed to the fact that DFT sometimes has limitations in mimicking weak dispersive interactions such as metallophilic interactions.[25] To justify the appropriateness of the method we currently employed in the calculations, a geometry optimization at the MP2 level of theory was also performed for the relatively smaller model complex **2a** with the constraint of C_{2v} symmetry, in which this method is believed to be able to reproduce the metallophilic interactions. Selected MP2 and PBE1PBE structural parameters of **2a**, together with the experimental parameters of **2**, are listed in Table S3 in the Supporting Information. All the calculated Cu−Cu distances in the MP2-optimized geometry of **2a** are found to be shorter than those in the experimental geometry of **2**. Although a slightly greater deviation from the experimental Cu−Cu distances was found in the PBE1PBE calculation than that in the MP2 calculation, the PBE1PBE-calculated structural parameters of **2a** are still in reasonable agreement with the experimental geometry of **2**. Considering the very high computational cost of the MP2 method for the size of our system and previous successful applications of DFT to the chemical and photophysical problems,[11] the present calculations using the PBE1PBE method should be appropriate and reliable in rationalizing the photophysical and fluxional behavior of this class of complexes.

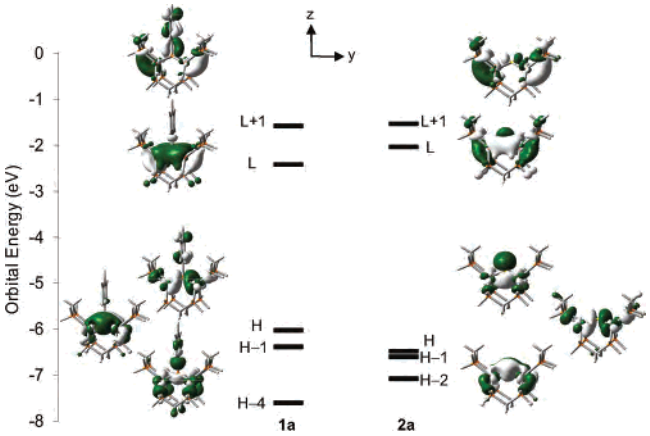

Figure 2. Spatial plots (isovalue 0.03) of selected frontier molecular orbitals (H, highest occupied; L, lowest unoccupied) of **1a** and **2a**.

Molecular Orbitals. To provide the framework for the singlet−singlet and singlet−triplet electronic excitations of the tetranuclear complexes **1a** and **2a**, their frontier molecular orbitals in CH_2Cl_2 have been examined. Figure 2 shows selected frontier molecular orbitals of **1a** and **2a**. The orbital compositions, which are expressed in terms of the contribution from the apical ligand E [E = PPh (**1a**), S (**2a**)], four Cu atoms (Cu), and four $H_2PCH_2PH_2$ ligands (dHpm), are listed in Table 1.

The HOMO, HOMO − 1, and HOMO − 4 of **1a** are the three high-lying molecular orbitals, consisting of the phosphorus 3p orbitals of the phosphinidene ligand mixed with Cu metal orbitals (Figure 2, left). Among these three high-lying molecular orbitals, the HOMO has the antibonding interaction between the $P(3p_y)$ orbital and the π_y orbital of

(24) Liu, C. W.; Hung, C.-M.; Santra, B. K.; Wang, J.-C.; Kao, H.-M.; Lin, Z. Y. *Inorg. Chem.* **2003**, *42*, 8551−8556.
(25) (a) Reimers J. R.; Cai Z.-L.; Biliæ A.; Hush, N. S. *Ann. N. Y. Acad. Sci.* **2003**, *1006*, 235−251. (b) Wang, S.-G.; Schwarz, W. H. E. *J. Am. Chem. Soc.* **2004**, *126*, 1266−1276.

Table 1. Calculated Percentage Contribution of the Selected Frontier MOs in **1a** and **2a**, Which Are Expressed in Terms of the Contribution from the Apical Ligand E [E = PPh (**1a**), S (**2a**)], Four Cu Atoms (Cu), and Four $PH_2CH_2PH_2$ Ligands (dHpm)

	E	Cu	dHpm
		1a	
LUMO + 1	15	50 (53, 40)[a]	35
LUMO	14	51 (1, 99)[a]	34
HOMO	35	45	19
HOMO − 1	36	50	14
HOMO − 2	10	51	39
HOMO − 3	46	30	24
HOMO − 4	20	51	29
		2a	
LUMO + 1	0	56 (43, 47)[a]	43
LUMO	4	56 (2, 93)[a]	40
HOMO	50	34	16
HOMO − 1	21	51	28
HOMO − 2	29	55	16

[a] Percent contributions of the Cu(4s, 4p) orbitals in parentheses.

Scheme 3. Simplified Pictures of the LUMO and LUMO + 1 of **1a**

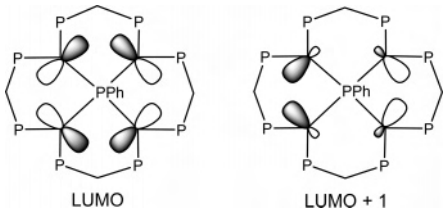

the phenyl ring, while the lowest energy HOMO − 4 has the P−C σ bonding interaction.

As listed in Table 1, the lowest unoccupied orbitals LUMO and LUMO + 1 are essentially metal-based, with some contribution from the $H_2PCH_2PH_2$ ligands. As shown in Figure 1, the copper atoms in the tetranuclear complexes are three-coordinated with two P atoms from two adjacent bridging dHpm ligands and one P atom from the phosphinidene ligand, forming a distorted trigonal planar geometry. Each copper atom can be considered to undergo an sp^2 hybridization, with an empty 4p orbital lying perpendicular to the CuP_3 plane. The LUMO is a metal bonding orbital, which is an in-phase combination of the empty Cu(4p) orbitals. The LUMO + 1 is also a metal bonding orbital, derived mainly from the Cu(4s) and Cu(4p) atomic orbitals. Scheme 3 illustrates the top view of the LUMO and the LUMO + 1 schematically.

The selected frontier molecular orbitals of **2a** are shown in Figure 2 (right). The first three highest occupied orbitals of **2a** consist of the sulfur 3p orbitals mixed with Cu metal orbitals. Similar to the LUMO and LUMO + 1 in **1a**, the LUMO and LUMO + 1 in **2a** are mainly metal-based (see Table 1 for the percent contribution of the molecular orbital of **2a**).

As depicted in Figure 2, the energies of the HOMO and HOMO − 1 in **1a** are higher than those of the corresponding orbitals in **2a**. The results can be related to the less electronegative character of the P atom, which makes the orbitals in **1a** higher lying. In addition, from Figure 2, the π_y orbital of the phenyl ring is antibonding with the P($3p_y$) orbital, which might further increase the HOMO energy of **1a** and hence decrease the HOMO−LUMO energy gap. Interestingly, a relatively low lying P($3p_z$) orbital (HOMO − 4) can be observed in **1a**. Presumably, the P($3p_z$) orbital is stabilized by its σ bonding with the phenyl group.

One can see that the LUMO of **1a** is lower in energy than that of **2a**. Since both the LUMOs in **1a** and **2a** are metal bonding orbitals, the LUMO energy can be affected by the Cu−Cu distances. The shorter average Cu−Cu distance for **1a** (3.090 Å) would make the LUMO slightly lower in energy relative to that for **2a** (3.093 Å).

Lowest Energy Singlet−Singlet Excitations. The photophysical data of **1** and **2** are listed in Table 2. The electronic absorption spectrum of **1** in CH_2Cl_2 at 298 K showed a low-energy absorption band at ca. 466 nm. However, the low-energy absorption band was blue-shifted in **2**, in which two shoulder peaks were found at ca. 354 and 402 nm. The low-lying singlet−singlet transitions of **1a** and **2a** based on their ground-state optimized geometries were computed by using the TDDFT approach (PBE1PBE) to provide insight into the nature of the electronic transitions. To take into account the solvent effect on the transition energies, the CPCM using CH_2Cl_2 as a solvent was applied together with TDDFT calculations.

Table 3 shows the transition energies to the low-lying singlet excited states in **1a** and **2a**. The transition energies to the first three low-lying excited states of **1a**, S_1, S_2, and S_3, calculated at 480, 419, and 354 nm, are mainly composed of HOMO → LUMO, HOMO − 1 → LUMO, and HOMO → LUMO + 1 excitations, respectively. Since the low-lying singlet−singlet transitions in **1a** involve the excitation from P(3p) orbitals mixed with Cu metal orbitals to the empty Cu−Cu bonding orbitals, the low-energy absorptions of **1** are probably attributed mainly to an admixture of an LMCT (PPh → Cu_4) transition and a metal-cluster-centered (MCC) [3d → 4s/3d → 4p] transition.

For **2a**, the first five singlet excited states consist of the excitation from S(3p) orbitals mixed with Cu metal orbitals to the empty Cu−Cu bonding orbitals, with their transition energies ranging from 311 to 360 nm. Similar to the origin assigned for the low-energy absorptions in **1**, the low-energy absorptions in **2** can also be assigned as LMCT (S → Cu_4)/MCC (3d → 4s/3d → 4p) singlet−singlet transitions.

In general, the calculated low-lying singlet−singlet transitions in **1a** and **2a** fall into the region of the low-energy absorption bands observed in the electronic absorption spectra of **1** and **2**. The low-lying singlet−singlet transitions (S_1 and S_2) in **1a** are calculated to be lower in energy than those in **2a**. This is in agreement with the experimental electronic absorption spectra in that the low-energy absorption band is blue-shifted from **1** to **2**. This is in line with the less electronegative character of the P atom, which has higher lying 3p orbitals and thus narrows the energy gap for the LMCT/MCC singlet−singlet transitions. Figure S1 of the Supporting Information shows a graphical representation of the experimental electronic absorption spectra of complexes **1** and **2** in dichloromethane at 298 K, as well as the calculated TDDFT singlet−singlet excitations with the oscillator strength (*f*) of complexes **1a** and **2a** shown in Table 3 for comparison.

Table 2. Photophysical Data for **1** and **2**

complex	medium (T/K)	λ_{abs}/nm (ϵ/dm^3 mol^{-1} cm^{-1})	λ_{em}/nm	λ_{ex}/nm	τ_o/μs
1	CH_2Cl_2 (298)	268 sh (49370), 316 sh (23460), 466 (3480)[a]	816[a]	339, 469[a]	2.0 ± 0.1[a]
	CH_2Cl_2 (77)		825[a]		330 ± 30[a]
	solid (298)		718[a]		8.3 ± 0.2[a]
	solid (77)		754[a]		550 ± 50[a]
2	CH_2Cl_2 (298)	270 (51500), 284 sh (47000), 354 sh (6650), 402 sh (2250)[b]	652[b]	350 sh, 371, 408 sh, 427 sh[b]	
	MeCN (298)	265 sh (41490), 285 sh (34650)[c]	618[c]		7.8 ± 0.2[c]
	^{n}PrCN (77)		539, 610 sh[c]		
	Me_2CO (298)		622[c]		8.1 ± 0.2[c]
	solid (298)		579[c]		3.6 ± 0.1[c]
	solid (77)		606[c]		

[a] From ref 9. [b] This work. [c] From ref 8a.

Table 3. TDDFT/CPCM (CH_2Cl_2) Vertical Excitation Energies [nm (eV)] for the Low-Lying Singlet Excited States with the Oscillator Strength (f) of Complexes **1a** and **2a**

complex	state	dominant excitation[a]	vertical excitation energy/nm (eV)	f
1a	S_1	HOMO → LUMO (0.7)	480 (2.58)	0.034
	S_2	HOMO − 1 → LUMO (0.7)	419 (2.96)	0.032
	S_3	HOMO → LUMO + 1 (0.7)	354 (3.51)	0.031
2a	S_1	HOMO − 1 → LUMO (0.7)	360 (3.45)	0.037
	S_2	HOMO → LUMO (0.7)	355 (3.49)	0.000
	S_3	HOMO − 2 → LUMO (0.7)	316 (3.92)	0.039
	S_4	HOMO → LUMO + 1 (0.7)	311 (3.99)	0.079
	S_5	HOMO − 1 → LUMO + 1 (0.6)	311 (3.99)	0.007

[a] Dominant excitations with the transition coefficients in parentheses.

At this point, one might argue that the calculated low-lying singlet−singlet transitions for the model complexes **1a** and **2a** cannot adequately describe the low-energy absorption bands in the electronic absorption spectra of **1** and **2**, as the phenyl groups of the diphosphine ligands might contribute considerably to these transitions, which would affect the conclusion that we arrived at. In view of this, single-point calculations using the same basis set and level of theory have been performed on model complexes by replacing one of the two hydrogen atoms on each of the eight phosphorus atoms of the diphosphines in the optimized structures of **1a** and **2a** with a phenyl ring under the constraint of a C_{2v} symmetry. The results showed that the two HOMOs (HOMO, HOMO − 1) and the two LUMOs (LUMO, LUMO + 1) in the phenyl-substituted models were also mainly composed of the 3p orbitals of the E ligand mixed with Cu metal orbitals and Cu−Cu metal bonding orbitals, respectively. More importantly, the phenyl groups of the diphosphines were found to contribute insignificantly to these frontier orbitals, suggesting their insignificant involvement in the low-energy transitions and hence further establishing the validity of the models used in the present study.

Lowest Triplet Excited States. The observation of luminescence lifetimes of complexes **1** and **2** in the microsecond range indicates that both emissions originate from excited states of triplet parentage (Table 2). The first two low-lying triplet excited states of **1a** and **2a** were calculated using TDDFT/CPCM(CH_2Cl_2) on the basis of their ground-state optimized geometries (Table 4). For complexes **1a** and **2a**, transitions to the T_1 and T_2 states involve mainly HOMO → LUMO and HOMO − 1 → LUMO excitations, respectively, in which these transitions can be described as predominantly LMCT (E → Cu_4)/MCC (3d → 4p) singlet−triplet transitions. On the basis of the result from TDDFT, the lowest energy triplet states in **1a** and **2a** involving populations via HOMO → LUMO excitation were optimized by using unrestricted UPBE1PBE to examine the structural changes of the lowest energy triplet states away from their corresponding ground states. As both the T_1 and T_2 states of **2a** are very close in energy, in which they only differ by 0.08 eV, optimization of the T_2 state involving HOMO − 1 → LUMO excitation has also been performed to establish the energy order of the two triplet states at relaxed molecular geometries.

Table 4. TDDFT/CPCM (CH_2Cl_2) Vertical Excitation Energies [nm (eV)] for the First Two Low-Lying Triplet Excited States of Complexes **1a** and **2a**

complex	state	dominant excitation[a]	vertical excitation energy/nm (eV)
1a	T_1	HOMO → LUMO (0.7)	517 (2.40)
	T_2	HOMO − 1 → LUMO (0.7)	463 (2.68)
2a	T_1	HOMO → LUMO (0.7)	385 (3.22)
	T_2	HOMO − 1 → LUMO (0.7)	376 (3.30)

[a] Dominant excitations with the transition coefficients in parentheses.

Optimizations of the lowest triplet state involving HOMO → LUMO excitation in **1a** with no symmetry constraint led to a significant structural distortion relative to the structure of its ground state. Figure 3 shows selected structural parameters of the optimized lowest triplet excited state in **1a** and the change in the structural parameters relative to those of the ground state. As depicted, large changes in the Cu−Cu distances are observed. The Cu(1)−Cu(1′) and Cu(2)−Cu(2′) distances are significantly shortened by 0.616 Å, compared to those of the ground-state geometry. Such distortion can be viewed as the contraction of the rectangular Cu_4 core.

Inspection of the two SOMOs of the optimized triplet excited state in Figure 4a reveals that the lower energy SOMO consists of the P($3p_y$) orbital mixed with the π_y orbital of the phenyl ring and the Cu metal orbitals, while the higher energy SOMO is mainly the in-phase combination of the empty Cu(4p) orbitals. Upon the population of electron density in this metal bonding orbital, it is expected that the Cu_4 rectangle is contracted. Such results indicate that the lowest triplet state of **1a** possesses predominantly both ^{3}LMCT (PPh → Cu) and ^{3}MCC (3d → 4p) character.

Geometry optimizations were performed on the two triplet excited states of **2a** without the symmetry constraint,

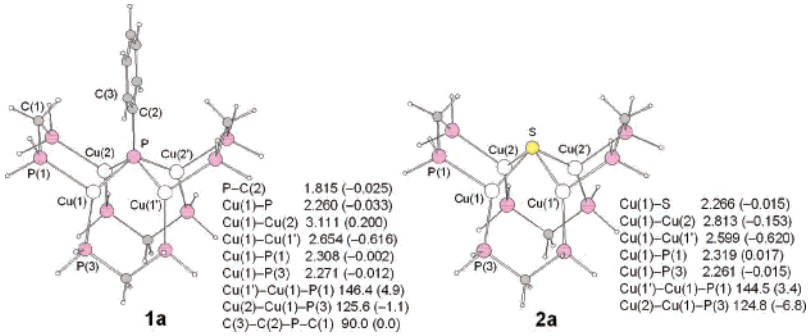

Figure 3. Selected structural parameters of the optimized lowest triplet excited states in **1a** and **2a** with the change in structural parameters with respect to those of the ground states in parentheses. Bond lengths and angles are in angstroms and degrees, respectively.

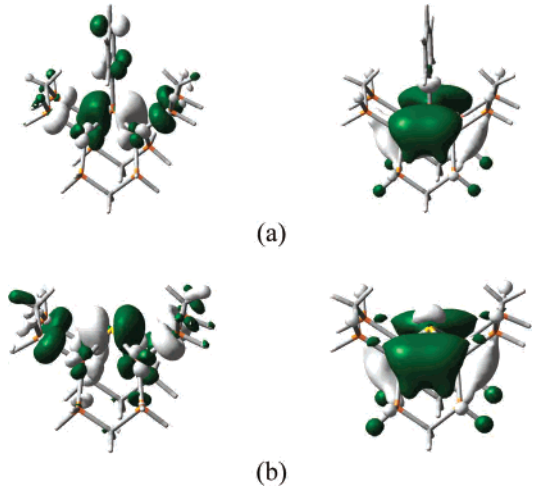

Figure 4. Spatial plots (isovalue 0.03) of the lower energy (left) and higher energy (right) SOMOs for **1a** (a) and **2a** (b) at their optimized lowest triplet excited states.

involving HOMO → LUMO and HOMO − 1 → LUMO excitations. Upon optimization, the HOMO − 1 → LUMO excited state is calculated to be 0.21 eV lower in energy than the HOMO → LUMO excited state. Since the HOMO − 1 → LUMO excited state is lower in energy than the HOMO → LUMO excited state, it is probably the state for emission.

Figure 3 shows the optimized geometry of the HOMO − 1 → LUMO excited state of **2a**. Similar to the lowest energy triplet state of **1a**, the HOMO − 1 → LUMO excited state in **2a** exhibits a significant structural distortion relative to the structure of the ground state, in which the contraction of the Cu_4 rectangle can also be observed. All the Cu−Cu distances are shortened in the excited state, with a greater change of the Cu(1)−Cu(1′) and Cu(2)−Cu(2′) distances. Two SOMOs of the triplet state from HOMO − 1 → LUMO excitation are shown in Figure 4b. The lower energy SOMO is mainly contributed by the S($3p_y$) orbital mixed with the Cu metal orbitals, while the higher energy SOMO is an in-phase combination of the empty Cu(4p) orbitals. Therefore, the lowest triplet state of **2a** contains mainly ^{3}LMCT (S → Cu)/^{3}MCC (3d → 4p) character.

On the basis of the calculated results of **1a** and **2a**, the origin of the emission in **1** and **2** can be assigned as derived from the triplet states consisting of the admixture of predominantly LMCT (E → Cu_4) and MCC (3d → 4p) characters. The theoretical emission maxima of the ^{3}LMCT/^{3}MCC excited states of **1a** and **2a**, estimated from the differences between the triplet- and ground-state energies at their corresponding excited-state equilibrium geometries in CH_2Cl_2, are 873 and 588 nm, respectively. The calculated emission maxima in **1a** and **2a** match well with the emission band at 816 and 655 nm in **1** and **2**, respectively. A red shift of the emission from **2** to **1** is also reflected from the calculations, and this shift can be attributed to the less electronegative nature of the P atom together with the presence of the phenyl group attached to the phosphinidene P in **1**, which results in a higher energy ligand orbital and a narrower energy gap for the emission.

Our results show that the optimized triplet states of complexes **1a** and **2a** exhibit a significant structural distortion involving the contraction of the Cu_4 rectangular base. The distorted ^{3}LMCT/^{3}MCC excited states can account for a large Stokes shift observed in complexes **1** (9067 cm^{-1}) and **2** (11617 cm^{-1}). Such distortion can also explain the observed rigidochromism of the emission band in **1** and **2**, since a more rigid medium would certainly increase the energy of such a highly distorted excited state.

NMR Fluxionality. As mentioned in the Introduction, the fluxionality which involved the exchange of the two types of diphosphines was only observed in **2** at both 298 and 233 K, but not in **1** at ambient temperature. The mechanism for the exchange process of **2a** was investigated to elucidate the fluxionality observed. Two possible mechanisms for the diphosphine exchange on **2a** were studied. One is related to the shuttling motion of the sulfido ligand through the Cu_4 unit (Scheme 2a), while the other involves the up−down flipping motion of the two pairs of diphosphines (Scheme 2b).

The transition state for the diphosphine exchange through the shuttling of the sulfido ligand was located and lies 0.5 kcal mol^{-1} above **2a**. Figure 1 shows the transition-state structure with D_2 symmetry. As depicted, all four Cu atoms form a square at an equal distance of 3.217 Å, with the S atom lying in the center of the Cu_4 plane. Vibrational frequency calculation shows one imaginary frequency (35*i* cm^{-1}), which corresponds to the shuttling motion of the sulfido ligand. An intrinsic reaction coordinate (IRC)[26]

(26) Gonzalez, C.; Schlegel, H. B. *J. Phys. Chem.* **1990**, *94*, 5523−5527.

calculation was done to confirm the reaction pathway in both directions from the transition state leading to **2a**.

Attempts to optimize a transition state for the diphosphine exchange via the up−down flipping of diphosphines were not successful, due to the complicated motions involved for the flipping of the diphosphines. However, we envisage that the up−down flipping process can be considered as the flattening of the four diphosphine flaps toward the Cu_4 plane. In this regard, an energy of **2a** with a geometry that is slightly distorted in such a way that the eight Cu−Cu−P angles[27] open up by 10°, i.e., the four diphosphine flaps are folded toward the Cu_4 plane, was determined. This distorted state was found to be 2.3 kcal mol^{-1} higher in energy than that for the optimized equilibrium geometry and also higher in energy than that required for the shuttling pathway. Besides, one would expect that the energy required for the actual up−down flipping motion in **2** should be even higher, simply because of the introduction of the 16 bulkier phenyl groups. The presence of these phenyl rings, however, should impose little influence on the shuttling motion. On the basis of the very small barrier calculated for the shuttling motion of the sulfido ligand, we believe that the exchange of the chemical environment for the diphosphines via the shuttling mechanism should be more feasible. The presence of facile exchange processes only in the sulfido complex but not in the phosphinidene counterpart is also in favor of the shuttling mechanism. Due to the larger bulk of the phosphinidene group, it is unlikely for **1** to undergo similar diphosphine exchange via the shuttling mechanism. One might think of a possibility that the exchange process in **2** can proceed via a mechanism that involves the dissociation of the bridging diphosphines. However, such a dissociation process is believed to be less likely as it should require a much higher energy compared to the calculated barrier (0.5 kcal mol^{-1}) for the shuttling motion of the sulfido ligand. This has been supported by the NMR study, in which no signal corresponding to the decoordination of the phosphine was observed.

Conclusion

The electronic structures of the ground and excited states for the luminescent tetranuclear copper(I) complexes $[Cu_4(\mu\text{-dppm})_4(\mu_4\text{-E})]^{2+}$ [E = PPh (**1**) and S (**2**)] were studied by using DFT calculations. The TDDFT calculations indicate that the lowest energy absorptions of both **1** and **2** are attributed mainly to the LMCT (E → Cu_4)/MCC (3d → 4s/3d → 4p) singlet−singlet transitions. The geometry optimizations on the lowest energy triplet state reveal that the emissive states of both complexes involve a considerable structural distortion in which they are derived predominantly from an admixture of ^{3}LMCT (E → Cu_4) and ^{3}MCC (3d → 4p) origin.

The mechanisms for the diphosphine exchange in **2** were investigated to account for the $^{31}P\{^1H\}$ NMR fluxionality observed in **2**. It is found that the exchange mechanism in the sulfido analogue involving the shuttling of the sulfido ligand through the Cu_4 plane, in which the transition state has the S atom lying in the plane of the Cu_4 square, is much more feasible compared to the mechanism that involves the up−down flipping of the two pairs of diphosphines. These results can explain the presence of facile exchange of the upper and lower diphosphine environments in the sulfido complex, but not in the phosphinidene counterpart due to the inaccessibility of the mechanism by the bulky phosphinidene group.

Acknowledgment. V.W.-W.Y. acknowledges support from the University Development Fund (UDF) of The University of Hong Kong, the URC Seed Funding for Strategic Research Theme on Organic Optoelectronics, and The University of Hong Kong Foundation for Educational Development and Research Ltd. W.H.L. acknowledges the support of a University Postdoctoral Fellowship, which is administered by The University of Hong Kong. We also thank Professor Zhenyang Lin from the Hong Kong University of Science and Technology for his helpful discussion on the theoretical studies and the Computer Center at The University of Hong Kong for providing the computational resources.

Supporting Information Available: UPBE1PBE electronic energies, selected MP2 and PBE1PBE structural parameters of **2a**, optimized geometries, and a plot of electronic absorption spectra of **1** and **2** with the calculated TDDFT singlet−singlet excitations of **1a** and **2a**. This material is available free of charge via the Internet at http://pubs.acs.org.

IC0612855

(27) An optimization was performed on **2a** with the constraint of the four upper Cu−Cu−P angles [Cu(1)−Cu(1′)−P(1′), Cu(1′)−Cu(1)−P(1), Cu(2)−Cu(2′)−P(2′), and Cu(2′)−Cu(2)−P(2)] and four lower Cu−Cu−P angles [Cu(2)−Cu(1)−P(3), Cu(2′)−Cu(1′)−P(3′), Cu(1)−Cu(2)−P(4), and Cu(1′)−Cu(2′)−P(4′)] to 151° and 142°, respectively, which are increased by 10° from those of the optimized ground-state geometries (see the labeling scheme in Figure 1).